

## TWO NEW OUTBURSTS AND TRANSIENT HARD X-RAYS FROM 1E 1048.1–5937

R.F. ARCHIBALD,<sup>1,2</sup> P. SCHOLZ,<sup>3</sup> V. M. KASPI,<sup>2</sup> S. P. TENDULKAR,<sup>2</sup> AND A. P. BEARDMORE<sup>4</sup>

<sup>1</sup>*Department of Astronomy and Astrophysics, University of Toronto 50 St. George Street, Toronto, ON M5S 3H4, Canada*

<sup>2</sup>*Department of Physics & McGill Space Institute, McGill University, 3600 University Street, Montreal QC, H3A 2T8, Canada*

<sup>3</sup>*Dunlap Institute of Astronomy and Astrophysics, University of Toronto, 50 St. George Street, Toronto, ON M5S 3H4, Canada*

<sup>4</sup>*Department of Physics and Astronomy, University of Leicester, University Road, Leicester LE1 7RH, UK*

### ABSTRACT

Since its discovery, 1E 1048.1–5937 has been one of the most active magnetars, both in terms of radiative outbursts, and changes to its spin properties. Here we report on a continuing monitoring campaign with the *Neil Gehrels Swift Observatory* X-ray Telescope in which we observe two new outbursts from this source. The first outburst occurred in 2016 July, and the second in 2017 December, reaching peak 0.5–10 keV absorbed fluxes of  $3.2_{-0.3}^{+0.2} \times 10^{-11}$  erg s<sup>-1</sup> cm<sup>-2</sup> and  $2.2_{-0.2}^{+0.2} \times 10^{-11}$  erg s<sup>-1</sup> cm<sup>-2</sup>, respectively, factors of  $\sim 5$  and  $\sim 4$  above the quiescent flux. Both new outbursts were accompanied by spin-up glitches with amplitudes of  $\Delta\nu = 4.47(6) \times 10^{-7}$  Hz and  $\Delta\nu = 4.32(5) \times 10^{-7}$  Hz, respectively. Following the 2016 July outburst, we observe, as for past outbursts, a period of delayed torque fluctuations, which reach a peak spin-down of  $1.73 \pm 0.01$  times the quiescent rate, and which dominates the spin evolution compared to the spin-up glitches. We also report an observation near the peak of the first of these outbursts with *NuSTAR* in which hard X-ray emission is detected from the source. This emission is well characterized by an absorbed blackbody plus a broken power law, with a power-law index above  $13.4 \pm 0.6$  keV of  $0.5_{-0.2}^{+0.3}$ , similar to those observed in both persistent and transient magnetars. The hard X-ray results are broadly consistent with models of electron/positron cooling in twisted magnetic field bundles in the outer magnetosphere. However the repeated outbursts and associated torque fluctuations in this source remain puzzling.

*Keywords:* pulsars:general; pulsars: individual: 1E 1048.1–5937; stars: magnetars

### 1. INTRODUCTION

1E 1048.1–5937, one of the original “anomalous X-ray pulsars” (AXPs; [Mereghetti & Stella 1995](#)), is now classified as part of a small class

of pulsars known as magnetars – neutron stars which display behavior thought to be powered by their immense magnetic fields. For a recent review of magnetars see e.g. [Kaspi & Beloborodov \(2017\)](#) or [Coti Zelati et al. \(2018\)](#). A list of known magnetars is available at the

Corresponding author: P. Scholz  
[paul.scholz@dunlap.utoronto.ca](mailto:paul.scholz@dunlap.utoronto.ca)

*McGill Online Magnetar Catalog* (Olausen & Kaspi 2014)<sup>1</sup>.

1E 1048.1–5937 was discovered as a persistent X-ray source, with a pulse period of 6.4 s, using the *Einstein X-ray Observatory* (Seward et al. 1986). In the following decade, 1E 1048.1–5937 was occasionally observed with various X-ray missions and, by the mid-1990s, it was noticed that the spin-down rate was variable by order unity (Mereghetti 1995). X-ray flux variability in 1E 1048.1–5937 was first noted by Mereghetti et al. (2004). Starting in 1997, 1E 1048.1–5937 was monitored regularly with the *Rossi X-ray Timing Explorer (RXTE)*, until the decommissioning of *RXTE* in 2012 (Kaspi et al. 2001; Gavriil & Kaspi 2004; Dib & Kaspi 2014), and was monitored on a regular basis (Archibald et al. 2015) with the *Neil Gehrels Swift X-ray Telescope (XRT)* until 2018.

During this long-term monitoring, 1E 1048.1–5937 has been one of the most active known magnetars. It has exhibited four long-term flux flares, as well as several magnetar-like bursts, and pulse profile changes. Perhaps the most striking behavior in 1E 1048.1–5937 is the dramatically changing spin-down rate, which seems to occur regularly following its radiative outbursts (Gavriil & Kaspi 2004; Dib & Kaspi 2014; Archibald et al. 2015). While many magnetars have been shown to have sudden timing changes associated with flux increases (e.g. Pons & Rea 2012; Dib & Kaspi 2014), the repeated observation of an increased and variable torque following each observed flux flare is as yet unexplained (Archibald et al. 2015). Counting the 2016 July outburst reported here, 1E 1048.1–5937 has now repeated this unusual behavior – an X-ray outburst followed by delayed torque oscillations – four times, each separated by  $\sim 1700$  days.

<sup>1</sup> [www.physics.mcgill.ca/~pulsar/magnetar/main.html](http://www.physics.mcgill.ca/~pulsar/magnetar/main.html)

Here we report on two X-ray outbursts and subsequent torque variations in 1E 1048.1–5937. The first of these in 2016 July occurred with a delay from the previous outburst consistent with that predicted by Archibald et al. (2015). The second outburst, in 2017 December, does not follow this timescale, however, as we show, it is less energetic than the major outbursts, and decays with a shorter timescale.

We also report the results of a new *NuSTAR* hard X-ray observation during the 2016 July outburst, wherein 1E 1048.1–5937 is detected above 20 keV, displaying the hard X-ray tail that is ubiquitous among the magnetar class.

## 2. OBSERVATIONS

### 2.1. *Swift* XRT Monitoring

1E 1048.1–5937 was monitored regularly with the *Swift*-XRT since 2011 July as part of a campaign to study several magnetars (see e.g. Scholz et al. 2014; Archibald et al. 2015, 2017). The XRT was operated in Windowed-Timing (WT) mode for all observations, having a time resolution of 1.76 ms, and only one dimension of spatial resolution.

Data were downloaded from the HEASARC *Swift* archive, reduced using the `xrtpipeline` standard reduction script, and time-corrected to the Solar System Barycenter using `HEASOFT v6.22`. Following this, we processed the data in the same manner described by Archibald et al. (2017).

Observations, typically 1–1.5 ks long, were taken in groups of three, with the first two observations within approximately 8 hours of each other and the third approximately a day later. This observation strategy was adopted due to the source’s prior unstable timing behavior, in which maintaining phase coherence using a longer cadence was only possible for several-month intervals (Kaspi et al. 2001; Dib et al. 2009). In total, 655 XRT observations total-

ing 1.0 Ms of observing time spanning 2011 July through 2018 April were analyzed in this work.

## 2.2. *NuSTAR* Observation

Following the detection of the first new outburst reported in §3.1, we received *NuSTAR* Director’s Discretionary Time (DDT) to observe 1E 1048.1–5937 in outburst. The *NuSTAR* observation (obsid 90202032002) was taken on 2016 August 5 (MJD 57605) with an exposure time of 55 ks.

*NuSTAR* data were reduced using the `nupipeline` scripts, using `HEASOFT v6.20` and time-corrected to the Solar System Barycenter. Source events were extracted within a  $1'$  radius around the centroid. Background regions were selected from the same detector as the source location, and spectra were extracted using the `nuproducts` script.

Using `grppha`, channels 0–35 ( $< 3$  keV) and 1935–4095 ( $> 79$  keV) were ignored, and all good channels were binned to have a minimum of one count per energy bin.

As shown in Figure 1, 1E 1048.1–5937 is clearly detected across the *NuSTAR* band, including at energies above 20 keV allowing the spectral analysis described in §3.2.

## 3. FLUX & SPECTRAL EVOLUTION

### 3.1. Long-term Evolution

Following the data reduction described in §2.1, we fit the XRT observations using an absorbed blackbody model.  $N_{\text{H}}$  was held constant at  $5.8 \times 10^{21} \text{ cm}^{-2}$ , the best-fit value for the source before the 2012 outburst. Observations within one day of each other were grouped for this analysis.

Several individual observations, most notably in 2012 November, are significantly elevated from the long-term trend. These are most likely due to catching 1E 1048.1–5937 during a period of post-burst tail emission lasting several kiloseconds, as reported by An et al. (2014).

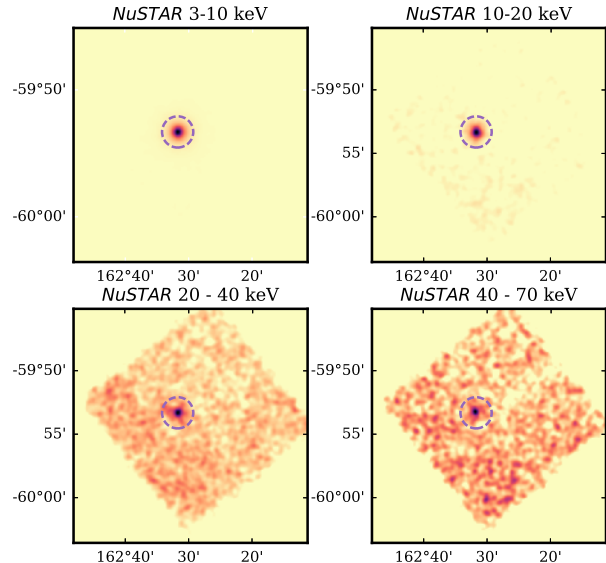


**Figure 1.** *NuSTAR* X-ray images in various energy bands of 1E 1048.1–5937 in outburst combining data from both focal plane modules. The images have been smoothed with a Gaussian with a width of 4 pixels ( $10''$ ). The position of 1E 1048.1–5937 is indicated by the dashed purple circle.

The long-term light-curve over the XRT campaign is dominated by three outbursts. We fit phenomenological models to the flux decay following each outburst, fixing the baseline flux to that measured before the 2011 December outburst, and fixing the outburst start time to that of the first observation with elevated flux. We first fit a single exponential decay, as well as power-law decays, to the flux following each outburst. For the first two long outbursts, such single-component models did not adequately describe the data.

When fitting two-component models, those consisting of exponentials were statistically preferred to power-law models, using  $\chi^2$  goodness of fit as a metric. The optimal parameters for a two-exponential model for each outburst are shown in Table 1.

For the 2017 December outburst, as the 2016 July outburst had not yet fully decayed, we sub-

**Table 1.** Characterization of the flux decay during the 2016 and 2017 outbursts of 1E 1048.1–5937.

| $t_b$ | 0.5–10 keV Flux Decay Fit $\star$  | $\chi^2_\nu$ |
|-------|--|--------------|
| MJD   | $10^{-11} \text{ erg s}^{-1} \text{ cm}^{-2}$  |              |
| 55926 | $(1.1 \pm 0.15) e^{-\frac{-(t-t_b)}{550 \pm 50}} + (1.9 \pm 0.13) e^{-\frac{-(t-t_b)}{50 \pm 10}}$ | 1.1          |
| 57592 | $(1.0 \pm 0.13) e^{-\frac{-(t-t_b)}{440 \pm 70}} + (1.5 \pm 0.16) e^{-\frac{-(t-t_b)}{51 \pm 9}}$  | 0.75         |
| 58120 | $\dagger (1.2 \pm 0.2) e^{-\frac{-(t-t_b)}{62 \pm 12}}$  | 1.5          |

$\star t$  and  $t_b$  are in units of days.

$\dagger$  After subtraction of the flux decay fit from the July 2016 outburst; see §3.1.

tracted the best-fit model of that latter outburst before fitting. As is evident from Figure 2, by the last observation reported here (2018 April), the effects of the 2017 December outburst have waned, with the last reported fluxes consistent with the extrapolation from the 2016 July outburst.

Note that for the two longest outbursts, both the short  $\sim 50$ - and long  $\sim 500$ -day exponential timescales are consistent at the  $1\sigma$  level with each other. In addition, the third outburst has a timescale consistent with the shorter  $\sim 50$ -day timescale. Also, within the limited available precision, the spectral variations are similar in the three outbursts (see Fig. 2).

### 3.2. Hard X-rays in Outburst

A *NuSTAR* observation was taken approximately 13 days after the *Swift*-XRT-detected flux increase, as indicated in Figure 2. We first verified that there were no short, magnetar-like bursts contaminating the data by conducting a burst search following the method described by Scholz & Kaspi (2011). To constrain the soft X-ray spectrum, we co-fit the *NuSTAR* observation with the *Swift* observations (observation ids 00032923252 & 254) taken on August 5–8 2016, coincident to within days of the epoch of the *NuSTAR* observation.

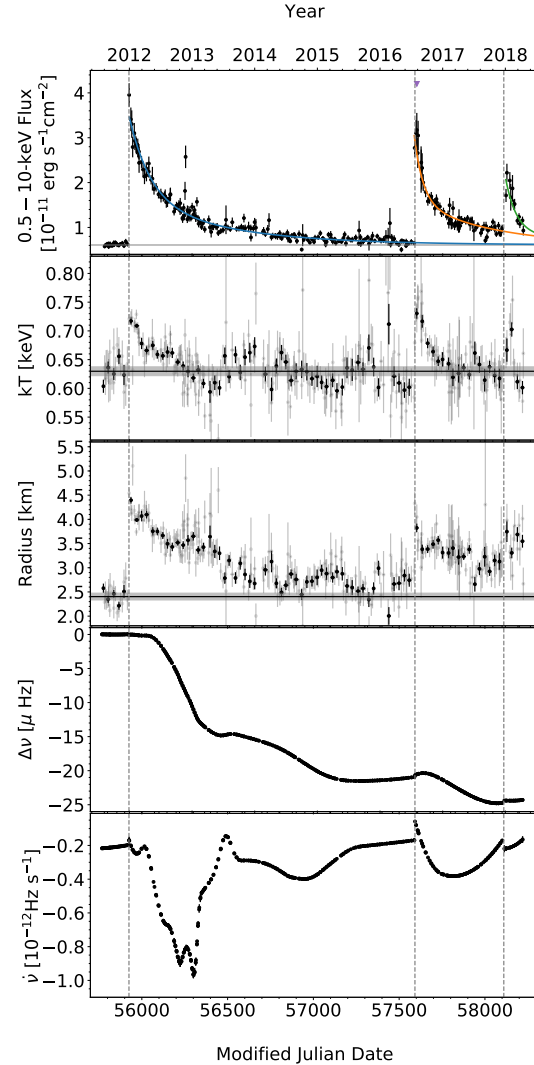


**Figure 2.** Flux and timing evolution of 1E 1048.1–5937 over the *Swift* campaign. The top panel shows the absorbed 0.5–10 keV X-ray flux. The purple triangle indicates the time of the *NuSTAR* observation. The best-fit models to the flux decays provided in Table 1 are shown as solid colored lines. The second and third panels show the evolution of the blackbody spectral parameters,  $kT$  and the radius, assuming a distance of 9 kpc (Durant & van Kerkwijk 2006). The light grey points show fits to observations grouped into days, and the black points combine observations into groups of one month. The bottom two panels show the evolution of the spin frequency,  $\nu$ , after the subtraction of the 2011 timing ephemeris, and that of the spin-down date,  $\dot{\nu}$ . The dashed vertical lines indicate the start of each outburst.

**Table 2.** *NuSTAR* & *Swift*-XRT spectrum of 1E 1048.1–5937 in outburst.

| Absorbed Blackbody & Broken Power-law   |                      |
|---|----------------------|
| Parameter                               | Value                |
| $N_{\text{H}}$ ( $10^{22}$ cm $^{-2}$ ) | $3.7 \pm 0.3$        |
| $C_{\text{NuSTAR}}^{\text{a}}$          | $0.85 \pm 0.05$      |
| $kT_{\text{BB}}$ (keV)                  | $0.88 \pm 0.02$      |
| $\Gamma_{\text{S}}$                     | $4.4 \pm 0.1$        |
| $\Gamma_{\text{H}}$                     | $0.5^{+0.3}_{-0.2}$  |
| Break Energy (keV)                      | $13.4^{+0.6}_{-0.6}$ |
| C-Stat/dof                              | 1809.7/1965          |
| Goodness $^{\text{b}}$                  | 49.7%                |
| Flux (0.5–10 keV) $^{\text{c}}$         | $31.2^{+0.7}_{-1.5}$ |
| Flux (3–79 keV) $^{\text{c}}$           | $20.^{+1}_{-2}$      |
| Flux (20–79 keV) $^{\text{c}}$          | $4.8^{+1.4}_{-1.2}$  |

$^{\text{a}}$ Fitted relative normalization for *NuSTAR*.

$^{\text{b}}$ Percentage of C-Stat statistic simulation trials from model parameters that are less than the fit statistic.

$^{\text{c}}$ Absorbed flux in units of  $10^{-12}$  erg cm $^{-2}$  s $^{-1}$ .

We used Cash statistics (Cash 1979) for fitting and parameter estimation of the unbinned data.  $N_{\text{H}}$  was fit using the `tbabs` model with `wilm` abundances (Wilms et al. 2000) and `vern` photoelectric cross-sections (Verner et al. 1996).

1E 1048.1–5937 is detected above 20 keV with a background subtracted 20–79-keV count rate of  $(5.3 \pm 0.6) \times 10^{-3}$  photons per second. The spectrum is well fit by an absorbed blackbody and broken power law; the best-fit parameters are shown in Table 2. Here,  $\Gamma_{\text{S}}$  and  $\Gamma_{\text{H}}$  refer to the power-law index below and above the break energy, respectively. The X-ray spectrum and residuals are shown in Figure 3. All the uncertainties in the spectral parameters are quoted at 90% confidence.

In a 2013 *NuSTAR* observation of 1E 1048.1–5937 in relative quiescence, neither Weng & Göğüş

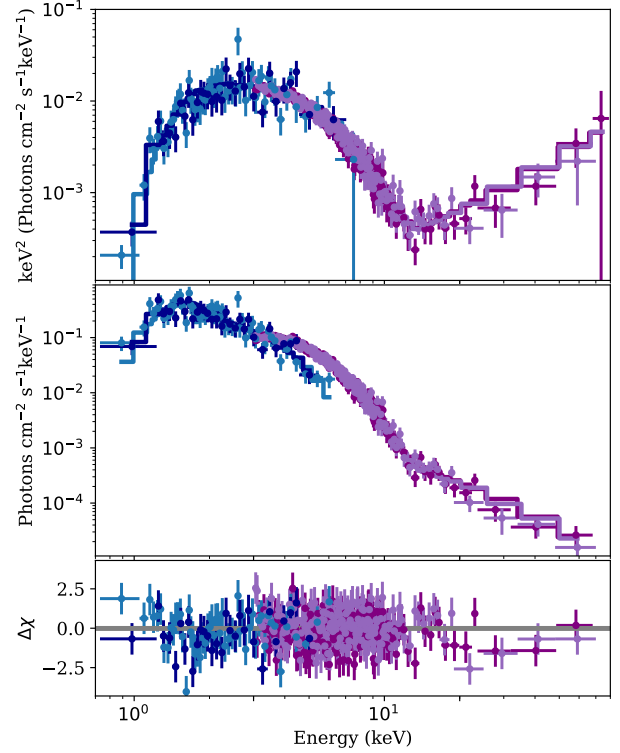


**Figure 3.** X-ray spectra of 1E 1048.1–5937 in outburst. In all panels, the blue data points are from *Swift*-XRT, and purple data points from *NuSTAR*. The top panel shows the spectral energy distribution, the middle panel shows the observed spectrum and the bottom panel displays the residuals of the data relative to the model presented in Table 2.

(2015) nor Yang et al. (2016) found any evidence of X-ray flux from 1E 1048.1–5937 above 20 keV, setting a  $3\sigma$  upper limit on the total, phase-averaged flux in the 20–79 keV band of  $\sim 3\text{--}4 \times 10^{-12}$  erg cm $^{-2}$  s $^{-1}$ , just below our detection of a flux of  $4.8^{+1.4}_{-1.2} \times 10^{-12}$  erg cm $^{-2}$  s $^{-1}$ .

### 3.3. *NuSTAR* Pulsed Flux

In Figure 4, we show the pulse profiles of 1E 1048.1–5937 during the *NuSTAR* observation in units of photons per kilosecond per Focal Plane Module (FPM), folded using the timing solution from the *Swift* campaign (see §4). We calculated the RMS pulsed fraction

**Table 3.** *NuSTAR* Pulsed Flux from 1E 1048.1–5937.

| Energy Range<br>keV | H-test $P_{FA}$     | RMS Pulsed Fraction†<br>% |
|---------------------|---------------------|---------------------------|
| 3–7                 | 0                   | $51 \pm 1$                |
| 7–10                | $1 \times 10^{-47}$ | $48 \pm 3$                |
| 10–13.4             | $1 \times 10^{-3}$  | $28 \pm 8$                |
| 13.4–20             | 0.03                | $30 \pm 10$               |
| 20–79               | 0.9                 | < 80                      |

† After background subtraction.

of 1E 1048.1–5937 in several energy bands, using the method described in the appendix of An et al. (2015). To determine the significance of the pulsed signal, we used the H-test (de Jager et al. 1989). Motivated by the spectral break in the power law at  $13.4^{+0.6}_{-0.6}$  keV, we used this value as a fiducial cut to search for a pulsed signal in the hard X-ray band. A pulsed signal is detected up to 20 keV, and no significant pulsations are seen above this energy. In Table 3 we report the H-test false-alarm-probabilities ( $P_{FA}$ ), and pulse fractions, where upper limits are given at the 99% confidence level. Due to a paucity of pulsed counts in the hard X-ray band, we can neither comment on the energy-dependence of the pulsed fraction, nor do meaningful phase-resolved spectroscopy of 1E 1048.1–5937.

#### 4. TIMING ANALYSIS

The processed individual XRT photons were used to derive a pulse time-of-arrival (TOA) for each observation. The rotational phase ( $\phi_i$ ) of every photon in the observation was calculated, assuming the best prior timing model. The TOAs were created using a Maximum Likelihood (ML) method as described by Livingstone et al. (2009) and Scholz et al. (2012).

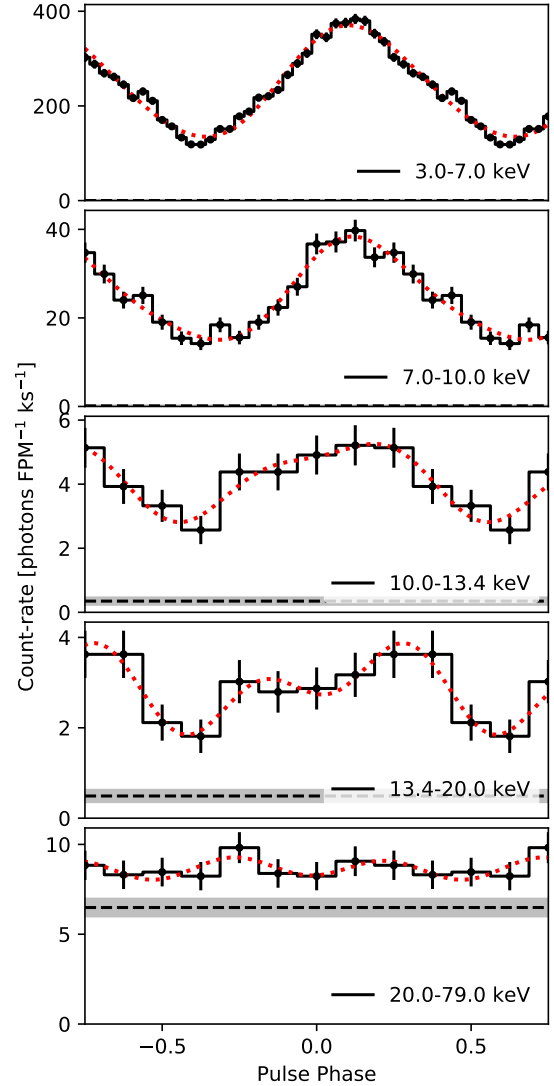


**Figure 4.** Pulse profile of 1E 1048.1–5937 in the *NuSTAR* observation in various energy bands. In all panels, the black dashed line represents the background count rate, and the red dashed line shows the H-test preferred pulse profile.

These TOAs were fitted to a timing model in which the phase  $\phi$  as a function of time  $t$  is described by a Taylor expansion:

$$\phi(t) = \phi_0 + \nu_0(t-t_0) + \frac{1}{2}\dot{\nu}_0(t-t_0)^2 + \frac{1}{6}\ddot{\nu}_0(t-t_0)^3 + \dots \quad (1)$$

where  $\nu$  is the rotational frequency of the pulsar. This was done using the *tempo2* pulsar timing software package (Hobbs et al. 2006).

As the frequency derivative of 1E 1048.1–5937 changes by up to an order of magnitude on  $\sim$ months time scales, we first created overlapping timing solutions with `tempo2` to determine a relative pulse number for each TOA. Then, using the overlapping regions to ensure the same number of rotations in each solution, these solutions were merged, allowing the establishment of absolute pulse numbers throughout the entire *Swift* campaign.

In order to determine the local timing behavior of 1E 1048.1–5937, we fit splines to these absolute pulse numbers (see [Dierckx 1975](#)), using a method similar to that described by [Dib & Kaspi \(2014\)](#), using piecewise polynomials of degree  $n = 3$  weighted by the inverse square error on the pulse phase. To determine uncertainties, we refit these splines 1000 times after adding Gaussian noise to the pulse numbers, using their measured pulse phase uncertainties. The resulting spin frequencies and frequency derivatives are shown in [Figure 2](#). The plotted error bars, typically comparable to the size of the points, indicate the 68% confidence regions.

We detected a spin-up glitch coincident with the 2016 July flux increase. As is evident in [Figure 2](#), the timing parameters of 1E 1048.1–5937 are not stable. To measure the size of the glitch, we fit a simple timing solution in the interval MJD 57400–57668, consisting of  $\nu$  and  $\dot{\nu}$  as well as a glitch in  $\nu$  with the epoch fixed to that of the flux increase. This yields a glitch with  $\Delta\nu = 4.47(6) \times 10^{-7}$  Hz ( $\Delta\nu/\nu = 2.89(4) \times 10^{-6}$ ). The above epoch bounds were chosen to have a reduced  $\chi^2 \sim 1$  and to result in no visible trends in the residuals. We note that the actual timing evolution is more complicated, as is evident in [Figure 2](#).

In the same manner, we also find a glitch coincident with the 2017 December flux increase. Fitting a simple timing solution in the interval MJD 58000–58200 with the epoch fixed to that of the flux increase gives a glitch having  $\Delta\nu =$

$4.32(5) \times 10^{-7}$  Hz ( $\Delta\nu/\nu = 2.79(3) \times 10^{-6}$ ). Again, note that the actual timing evolution is more complicated ([Fig. 2](#)).

The influence of these glitches on the long-term spin down of the pulsar is far smaller than the integrated effect of the varying torque. Collectively, the two glitches change  $\nu$  by  $\sim 8.8 \times 10^{-7}$  Hz while the added spin-down variations have contributed  $\sim -2 \times 10^{-5}$  Hz.

## 5. DISCUSSION

### 5.1. *Hard X-ray Component*

Here we have presented the detection of 1E 1048.1–5937 at energies above 20 keV. This, however, is not the first high energy detection of the source. [Leyder et al. \(2008\)](#) detected 1E 1048.1–5937 at 22–100 keV with *INTEGRAL* during observations of  $\eta$  Carinae. Their observation totals 1.1 Ms and is drawn from several observing epochs, but one of those epochs (MJD 52787–52827) corresponds to the peak of the 2001–2002 outburst of 1E 1048.1–5937. This is therefore consistent with the picture of 1E 1048.1–5937 being bright in hard X-rays during outburst.

Hard X-ray emission from magnetars is ubiquitous in persistently bright magnetars (e.g. [Kuiper et al. 2006](#); [Vogel et al. 2014](#); [Younes et al. 2017a](#); [Enoto et al. 2017](#)). Additionally, in transient magnetars, similar hard-X-ray components are observed near epochs of enhanced flux. For example, in SGR 0501+4516, for which, in the first four days of an outburst, *Suzaku* detected a hard power law with  $\Gamma = 0.79_{-0.18}^{+0.20}$  ([Enoto et al. 2010](#)) – similar to the spectrum we have observed in 1E 1048.1–5937. As well, in SGR 1935+2154 ([Younes et al. 2017b](#)), a hard X-ray component was observed at the peak flux of an outburst. Thus the phenomenon of a transient hard X-ray component appearing in outburst seems common for the magnetar class.

This hard X-ray emission is thought to be due to decelerating electron/positron flow in large

twisted magnetic loops of the pulsar magnetosphere (Beloborodov 2013). In this picture, the flux evolution of magnetars following outbursts involves the untwisting of the magnetosphere (e.g. Beloborodov 2009; Parfrey et al. 2013; Chen & Beloborodov 2017). The transient hard-X-ray emission we observed in 1E 1048.1–5937, and other magnetars in outburst, is then consistent with this picture where hard-X-ray emission is only detectable during the peak of this outburst when the magnetosphere is maximally twisted. We would then generally expect the evolution of the hard X-ray flux to proceed on a similar timescale to that of the soft X-ray flux (Chen & Beloborodov 2017). Future systematic hard X-ray observations of magnetars in outburst are needed to put this to the test, although the hard X-ray relaxation of the high-magnetic-field radio pulsar PSR J1119–6127 has recently been shown to proceed on a time scale similar to that of the soft X-ray relaxation post-outburst (Archibald et al. 2018).

A correlation has been observed between the surface magnetic field (or alternately the spin-down rate) of a magnetar and its hard X-ray power-law index (Kaspi & Boydston 2010; Enoto et al. 2017). Indeed, Kaspi & Boydston (2010) predicted that  $\Gamma_H$  for 1E 1048.1–5937 should fall between 0–1, albeit in quiescence. Interestingly, this is in agreement with our measurement of  $\Gamma_H = 0.5^{+0.3}_{-0.2}$  in outburst.

In Enoto et al. (2017), the hardness ratio of fluxes in the 15–60 keV and 1–10 keV bands is shown to be correlated with the spin-down rate of the magnetar. If we take the quiescent spin-down rate of 1E 1048.1–5937 ( $\sim 9 \times 10^{-12} \text{ s s}^{-1}$ ), the predicted hardness ratio for 1E 1048.1–5937 is  $\sim 0.4$ . We measure  $F_{15-60 \text{ keV}} = (3.2 \pm 0.6) \times 10^{-12} \text{ erg cm}^{-2} \text{ s}^{-1}$  and  $F_{1-10 \text{ keV}} = (31 \pm 1) \times 10^{-12} \text{ erg cm}^{-2} \text{ s}^{-1}$  for a hardness ratio of  $0.10 \pm 0.02$  which is broadly consistent with the trend, especially given the large fluctuations in  $\dot{P}$  observed in 1E 1048.1–5937, as well as the

scatter in the observed distribution (Enoto et al. 2017).

### 5.2. Repeated outbursts & torque changes in 1E 1048.1–5937

In Figure 5 we show the last 20 yr of evolution in the X-ray flux, and spin-down rate for 1E 1048.1–5937, as monitored by *RXTE*<sup>2</sup> and *Swift*. Note that the fluxes are in different energy bands (0.5–10 keV vs 2–20 keV), and that *RXTE* fluxes are pulsed only, and have been scaled to match the *Swift* flux during the period of overlap.

The time delay between the 2011 December and the 2016 July outbursts was  $1670 \pm 10$  days. This can be compared to separations of  $1800 \pm 10$  and  $1740 \pm 10$  days between the prior flares as discussed by Dib & Kaspi (2014) and Archibald et al. (2015). While this outburst timing is consistent with the quasi-periodicity suggested in Archibald et al. (2015), the occurrence of the 2017 December outburst suggests that this repeated time scale is spurious. However, this last outburst is decaying on a faster timescale than the major outbursts on which the claimed quasi-periodicity is based – similar to the precursor flare noted in 2001 (e.g. Tam et al. 2008; Dib & Kaspi 2014). It will be interesting to continue monitoring 1E 1048.1–5937 to see if there is another outburst on the timescale the quasi-periodicity predicts, i.e. in  $\sim 2021$ .

Additionally, the torque variations following the 2016 July outburst follow the trend of decreasing amplitude noted in Archibald et al. (2015). Following the four major outbursts observed thus far, the peak torque reached values of 12.3(1), 7.32(5), 4.4(1), and finally 1.73(1) times higher than the quiescent rate. The monotonic decrease in amplitude of these unexplained torque variations is curious, as it im-

<sup>2</sup> The *RXTE* data presented here are reproduced from Dib & Kaspi (2014), with the timing solutions pre-2000 from Kaspi et al. (2001).

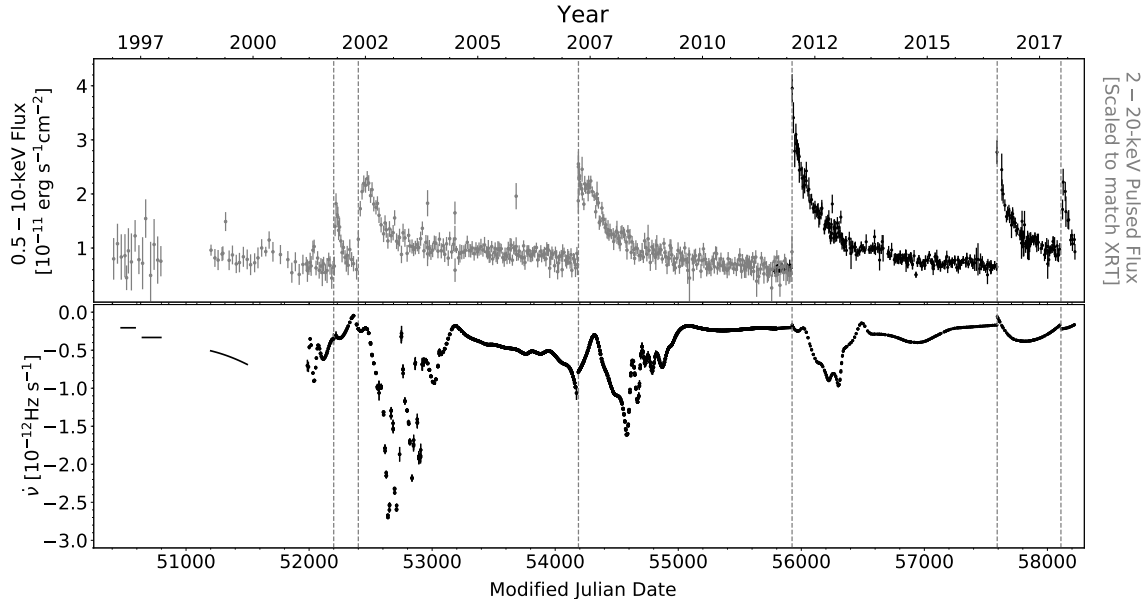


**Figure 5.** Flux and timing evolution of 1E 1048.1–5937 over the combined *RXTE* and *Swift* campaigns. The top panel shows the absorbed 0.5–10 keV X-ray flux in black, and the *RXTE* 2–20 keV pulsed flux measured with the proportional counter array (Jahoda et al. 1996) in grey, scaled to match the *Swift* total flux. The bottom panel shows the evolution of the spin-down date,  $\dot{\nu}$ . In both panels, the dashed vertical lines indicate the start of a flux increase. The *RXTE* data are from Dib & Kaspi (2014), with the timing solutions pre-2000 from Kaspi et al. (2001).

plies that our monitoring of 1E 1048.1–5937 was started at a special time, perhaps after a major but unobserved event. If the decline continues, by the next outburst, the torque variations should be smaller than order unity times the quiescent value. However, the monotonic decrease may also be purely coincidental. Further monitoring will be illuminating.

While the repetition, and monotonic decline in amplitude, of the torque variations from 1E 1048.1–5937 are striking and unique, rapid, extreme variability in the torque ( $\dot{\nu}$ ) evolution appears to be a common feature following magnetar outbursts. In addition to that observed now repeatedly in 1E 1048.1–5937, similar variations have been observed in 1E 1547–5408 (Dib et al. 2012), PSR J1622–4950 (Scholz et al. 2017; Camilo et al. 2018), and in XTE 1810–197 (Camilo et al. 2016). Thus, in a large fraction of magnetar outbursts for which the spin-down rate has been tracked for over a decade, these extreme torque variations are observed, and can

dominate the long-term spin evolution of these sources.

In the magnetar model, increased torque associated with outbursts, just as the enhanced hard X-ray emission, is due to a twist in the magnetosphere (e.g Thompson et al. 2002; Beloborodov 2009). As the spin-down rate of the star is dominated by the relatively small number of open field lines, there is no reason for a strict correlation between the hard X-ray emission and spin-down rate, as it depends on the geometry of the magnetosphere (Beloborodov 2009; Kaspi & Beloborodov 2017). In the untwisting model, the spin-down rate of the star is only affected once the twist reaches an amplitude of  $\sim 1$  radian. The delay between the peak X-ray flux and peak torque of  $\sim 100$  days observed in 1E 1048.1–5937 would then be due to the initial twist not exceeding this threshold value (Beloborodov 2009).

## 6. CONCLUSIONS

We have presented long-term X-ray observations of 1E 1048.1–5937 during which we observe two new outbursts of this source in 2016 July and 2017 December. Associated with these outbursts, we find spin-up glitches having  $\Delta\nu/\nu$  of order  $10^{-6}$ , although the long-term spin evolution is dominated by a strongly fluctuating spin-down rate. We also report a transient hard X-ray component of 1E 1048.1–5937 observed with *NuSTAR* near the peak of the 2016 July outburst, with emission up to  $\sim 70$  keV, and pulsed emission observed up to 20 keV. The spectrum and pulse properties of this hard emission are qualitatively consistent with emission models involving cooling of electron/positron pairs in large, twisted magnetic loops in the outer regions of the stellar magnetosphere (Beloborodov 2013). The repeating outbursts and associated large, delayed torque variations, and their possible monotonic decline in amplitude in 1E 1048.1–5937 remain, however, puzzling.

R.F.A. acknowledges support from an NSERC Postdoctoral Fellowship. P.S. is a Dunlap Fellow and an NSERC Postdoctoral Fellow. The Dunlap Institute is funded through an endowment established by the David Dunlap family and the University of Toronto. V.M.K. receives support from an NSERC Discovery Grant and Herzberg Award, the Centre de

Recherche en Astrophysique du Québec, an R. Howard Webster Foundation Fellowship from the Canadian Institute for Advanced Study, the Canada Research Chairs Program and the Lorne Trottier Chair in Astrophysics and Cosmology. A.P.B. acknowledges funding from the UK Space Agency. The authors thank the operations team of *NuSTAR* for approving a rapid turn-around DDT. We thank the *Swift* team for approving our ToO requests to monitor 1E 1048.1–5937, and other magnetars over the years. This research has made use of data obtained through the High Energy Astrophysics Science Archive Research Center Online Service, provided by the NASA/Goddard Space Flight Center. This work made use of data from the *NuSTAR* mission, a project led by the California Institute of Technology, managed by the Jet Propulsion Laboratory, and funded by the National Aeronautics and Space Administration.

*Facilities:* *NuSTAR*, *Swift*

*Software:*

`numpy` (van der Walt et al. 2011),  
`astropy` (Astropy Collaboration et al. 2013, 2018),  
`xspec` (Arnaud 1996),  
`heasoft` (HEASARC 2014)

## REFERENCES

- An, H., Kaspi, V. M., Beloborodov, A. M., et al. 2014, *ApJ*, 790
- An, H., Archibald, R. F., Hascoët, R., et al. 2015, *ApJ*, 807, 93
- Archibald, R. F., Kaspi, V. M., Ng, C.-Y., et al. 2015, *ApJ*, 800, 33
- Archibald, R. F., Kaspi, V. M., Scholz, P., et al. 2017, *ApJ*, 834, 163
- Archibald, R. F., Kaspi, V. M., Tendulkar, S. P., & Scholz, P. 2018, *ApJ*, 869, 180
- Arnaud, K. A. 1996, in *Astronomical Society of the Pacific Conference Series*, Vol. 101, *Astronomical Data Analysis Software and Systems V*, ed. G. H. Jacoby & J. Barnes, 17
- Astropy Collaboration, Robitaille, T. P., Tollerud, E. J., et al. 2013, *A&A*, 558, A33
- Astropy Collaboration, Price-Whelan, A. M., Sipőcz, B. M., et al. 2018, *AJ*, 156, 123
- Beloborodov, A. M. 2009, *ApJ*, 703, 1044
- . 2013, *ApJ*, 762, 13
- Camilo, F., Ransom, S. M., Halpern, J. P., et al. 2016, *ApJ*, 820, 110

- Camilo, F., Scholz, P., Serylak, M., et al. 2018, *ApJ*, 856, 180
- Cash, W. 1979, *ApJ*, 228, 939
- Chen, A. Y., & Beloborodov, A. M. 2017, *ApJ*, 844, 133
- Coti Zelati, F., Rea, N., Pons, J. A., Campana, S., & Esposito, P. 2018, *MNRAS*, 474, 961
- de Jager, O. C., Raubenheimer, B. C., & Swanepoel, J. W. H. 1989, *A&A*, 221, 180
- Dib, R., & Kaspi, V. M. 2014, *ApJ*, 784, 37
- Dib, R., Kaspi, V. M., & Gavriil, F. P. 2009, *ApJ*, 702, 614
- Dib, R., Kaspi, V. M., Scholz, P., & Gavriil, F. P. 2012, *ApJ*, 748
- Dierckx, P. 1975, *J.Comp.Appl.Maths*, 1, 165
- Durant, M., & van Kerkwijk, M. H. 2006, *ApJ*, 650, 1070
- Enoto, T., Rea, N., Nakagawa, Y. E., et al. 2010, *ApJ*, 715, 665
- Enoto, T., Shibata, S., Kitaguchi, T., et al. 2017, *The Astrophysical Journal Supplement Series*, 231
- Gavriil, F. P., & Kaspi, V. M. 2004, *ApJ*, 609, L67
- HEASARC. 2014, HEASoft: Unified Release of FTOOLS and XANADU, ascl:1408.004
- Hobbs, G. B., Edwards, R. T., & Manchester, R. N. 2006, *MNRAS*, 369, 655
- Jahoda, K., Swank, J. H., Giles, A. B., et al. 1996, in *Society of Photo-Optical Instrumentation Engineers (SPIE) Conference Series*, Vol. 2808, EUV, X-Ray, and Gamma-Ray Instrumentation for Astronomy VII, ed. O. H. Siegmund & M. A. Gummin, 59
- Kaspi, V. M., & Beloborodov, A. M. 2017, *ARA&A*, 55, 261
- Kaspi, V. M., & Boydston, K. 2010, *ApJ*, 710, L115
- Kaspi, V. M., Gavriil, F. P., Chakrabarty, D., Lackey, J. R., & Munro, M. P. 2001, *ApJ*, 558, 253
- Kuiper, L., Hermsen, W., den Hartog, P. R., & Collmar, W. 2006, *ApJ*, 645, 556
- Leyder, J. C., Walter, R., & Rauw, G. 2008, *A&A*, 477, L29
- Livingstone, M. A., Ransom, S. M., Camilo, F., et al. 2009, *ApJ*, 706, 1163
- Mereghetti, S. 1995, *ApJ*, 455, 598
- Mereghetti, S., & Stella, L. 1995, *ApJL*, 442, L17
- Mereghetti, S., Tiengo, A., Stella, L., et al. 2004, *ApJ*, 608, 427
- Olausen, S. A., & Kaspi, V. M. 2014, *ApJS*, 212, 6
- Parfrey, K., Beloborodov, A. M., & Hui, L. 2013, *ApJ*, 774, 92
- Pons, J. A., & Rea, N. 2012, *ApJL*, 750, L6
- Scholz, P., Archibald, R. F., Kaspi, V. M., et al. 2014, *ApJ*, 783, 99
- Scholz, P., & Kaspi, V. M. 2011, *ApJ*, 739, 94
- Scholz, P., Ng, C.-Y., Livingstone, M. A., et al. 2012, *ApJ*, 761, 66
- Scholz, P., Camilo, F., Sarkissian, J., et al. 2017, *ApJ*, 841, 126
- Seward, F. D., Charles, P. A., & Smale, A. P. 1986, *ApJ*, 305, 814
- Tam, C. R., Gavriil, F. P., Dib, R., et al. 2008, *ApJ*, 677
- Thompson, C., Lyutikov, M., & Kulkarni, S. R. 2002, *ApJ*, 574, 332
- van der Walt, S., Colbert, S. C., & Varoquaux, G. 2011, *Computing in Science and Engineering*, 13, 22
- Verner, D. A., Ferland, G. J., Korista, K. T., & Yakovlev, D. G. 1996, *ApJ*, 465, 487
- Vogel, J. K., Hascoët, R., Kaspi, V. M., et al. 2014, *ApJ*, 789
- Weng, S.-S., & Göğüş, E. 2015, *ApJ*, 815, 15
- Wilms, J., Allen, A., & McCray, R. 2000, *ApJ*, 542, 914
- Yang, C., Archibald, R. F., Vogel, J. K., et al. 2016, *ApJ*, 831, 80
- Younes, G., Baring, M. G., Kouveliotou, C., et al. 2017a, *ApJ*, 851
- Younes, G., Kouveliotou, C., Jaodand, A., et al. 2017b, *ApJ*, 847